

**Studying Anomalous $WW\gamma$ and WWZ Couplings
with Polarized $p\bar{p}$ Collisions**

Michael Wiest, Daniel R. Stump, Douglas O. Carlson, C.-P. Yuan

Department of Physics and Astronomy

Michigan State University

East Lansing, MI 48824

Abstract

We calculate tree-level cross-sections for $W^+\gamma$ and W^+W^- production in proton-antiproton collisions, with one W decaying to leptons, with anomalous electroweak triple-boson coupling parameters $\Delta\kappa$ and λ . We compare the unpolarized cross-sections to those for a polarized proton beam, to study how a polarized proton beam would improve experimental tests of anomalous couplings.

PACS numbers: 11.15.-q, 11.80.Cr, 12.15.-y, 12.15.Ji, 12.20.Fv

1 Introduction

In the last few years the SPIN collaboration has shown in various technical notes that it is feasible to polarize the proton beam, longitudinally or transversely, during the colliding mode of the Tevatron [1]. Taking proton polarization as a possibility, we examine one of the possible physics topics that could be pursued with such a beam configuration – to study tri-boson couplings of the weak gauge bosons. (Other interesting physics topics involving polarization at the Tevatron collider can be found in Ref. [2].)

An important test of the electroweak Standard Model is to measure the couplings among gauge fields. In this paper we are concerned with the $WW\gamma$ and WWZ couplings. Let $W^\mu(x)$, $Z^\mu(x)$, and $A^\mu(x)$ denote the fields of W^- , Z^0 , and γ ; then the interaction Lagrangian we consider is

$$\begin{aligned} \mathcal{L}_3 = & -ig(W_{\mu\nu}^\dagger W^\mu - W_{\mu\nu} W^{\dagger\mu})(A^\nu \sin\theta_W + Z^\nu \cos\theta_W) \\ & -igW_\mu^\dagger W_\nu(A^{\mu\nu}\kappa_\gamma \sin\theta_W + Z^{\mu\nu}\kappa_Z \cos\theta_W) \\ & -\frac{ig}{M_W^2}W_{\mu\alpha}^\dagger W_\nu^\alpha(A^{\mu\nu}\lambda_\gamma \sin\theta_W + Z^{\mu\nu}\lambda_Z \cos\theta_W) \end{aligned} \quad (1)$$

where $A_{\mu\nu} = \partial_\mu A_\nu - \partial_\nu A_\mu$, *etc.* \mathcal{L}_3 is gauge invariant with respect to U(1) electromagnetic gauge transformations. The parameter κ_γ is the anomalous magnetic moment of the W^- , as defined by Lee and Yang [3]; λ_γ is an anomalous electric quadrupole moment. The parameters κ_Z and λ_Z are similar WWZ couplings. In the Standard SU(2) \times U(1) gauge theory these coupling parameters have the definite values

$$\kappa_\gamma = \kappa_Z = 1, \quad \lambda_\gamma = \lambda_Z = 0 \quad (\text{Standard Model}). \quad (2)$$

We define $\Delta\kappa$ by

$$\Delta\kappa = \kappa - 1. \quad (3)$$

If $\Delta\kappa$ or λ is significantly different than 0 for either γ or Z^0 , then the Standard $SU(2)\times U(1)$ gauge theory is not the complete theory of the electroweak interactions. In the Standard Model, $\Delta\kappa$ and λ can be induced at loop level, but only of the size of $\mathcal{O}(g^2/16\pi^2)$ at one-loop level from naive dimensional analysis [4]. Thus setting experimental limits on the anomalous $WW\gamma$ or WWZ couplings is an important test of the Standard Model; actually discovering large anomalous interactions would be a sign of new physics. We treat \mathcal{L}_3 as an effective Lagrangian and only use it for tree-level calculations.

To determine the WWV couplings (where V stands for γ or Z^0) it is necessary to measure the experimental cross-section, or the distribution of some kinematic variable, for a process that depends on the WWV coupling, and compare the measurement to a calculated prediction. In this paper we consider two processes in proton-antiproton collisions

$$p + \bar{p} \rightarrow W^+ \left(\rightarrow \ell^+ \nu_\ell \right) + \gamma ,$$

$$p + \bar{p} \rightarrow W^\pm \left(\rightarrow \ell^\pm \bar{\nu}_\ell \right) + W^\mp \left(\rightarrow 2 \text{ jets} \right) .$$

For ℓ we include both e and μ . The unpolarized cross-section for $p\bar{p} \rightarrow W^-\gamma$ is equal to that for $p\bar{p} \rightarrow W^+\gamma$ in a CP invariant theory such as \mathcal{L}_3 ; however, we are interested in polarized scattering, for which $W^+\gamma$ is more interesting than $W^-\gamma$ for a $p\bar{p}$ collider with a polarized proton beam.

The purpose of this paper is to explore the experimental search for anomalous couplings in proton-antiproton collisions, *assuming the protons are longitudinally polarized*. The antiprotons are assumed to be unpolarized. With the Tevatron collider in mind [1, 2], we consider the center-of-mass energy equal to 2 TeV.

The reaction cross-section for a process involving the $WW\gamma$ or WWZ coupling depends on the longitudinal polarization of the proton through spin-dependent parton

distribution functions. The coupling of W^\pm to quarks (ud or other flavor combinations) is a V–A interaction, so the parton-level cross-section depends strongly on the helicities of the quarks: for massless quarks a W^\pm couples only to left-handed (L) quarks and right-handed (R) antiquarks. Thus the parton-level process depends strongly on helicity. The question is whether the *proton process* depends strongly on proton helicity. If a polarized proton contained equal parton densities of left-handed and right-handed quarks, then the proton cross-section would not depend on the proton helicity. However, we know that the densities of L and R quarks are not equal for polarized protons. Therefore, the $p\bar{p}$ cross-section will be different for left-polarized and right-polarized protons.

Our calculations of the polarized-proton cross-sections depend on polarized parton distribution functions (hereafter abbreviated ppdf's), and these are only known with limited accuracy. The ppdf's are defined as follows: For any parton type f , we define

$$f_+(x) = \frac{1}{2}(f(x) + \Delta f(x)) \tag{4}$$

= density of L (or R) parton in L (or R) proton ,

$$f_-(x) = \frac{1}{2}(f(x) - \Delta f(x)) \tag{5}$$

= density of L (or R) parton in R (or L) proton ,

where x is the momentum fraction of the parton. There are nine different parton types

$$f = u_{val} , d_{val} , u_{sea} = \bar{u}_{sea} , d_{sea} = \bar{d}_{sea} , g , s = \bar{s} , c = \bar{c} , b = \bar{b} , t = \bar{t} . \tag{6}$$

In the ppdf's we used, the u and d sea distributions are equal, but different than the s and c distributions, and the b and t distributions are zero

$$u_{sea}(x) = d_{sea}(x) ; b(x) = 0 ; t(x) = 0 . \tag{7}$$

Figure 1.1 shows the polarization dependence of the ppdf's we used, by plotting $x \Delta f(x)$ for several parton species. The ppdf's depend on momentum scale Q ; *i.e.* $f_{\pm} = f_{\pm}(x, Q^2)$. Fig. 1.1 corresponds to $Q=80$ GeV. (These ppdf's are calculated from a program based on Morfin-Tung parton distribution functions [5, 6].) The ppdf's have been measured, to some limited precision, from polarized deep-inelastic lepton scattering [7]. Recent data from the Spin Muon Collaboration (SMC) at CERN provide a measurement of the polarization difference, integrated over x and weighted by e_q^2/e^2 [8]:

$$I \equiv \int_0^1 dx \sum_{f=u,d,s,c} \frac{e_f^2}{e^2} \frac{1}{2} [\Delta f(x, Q^2) + \Delta \bar{f}(x, Q^2)] \quad (8)$$

$$= 0.142 \pm 0.008 \pm 0.011,$$

where the momentum scale is $Q^2 = 10 \text{ GeV}^2$. The ppdf's used in our calculations have

$$I = 0.138 \text{ for } Q^2 = 10 \text{ GeV}^2, \quad (9)$$

$$I = 0.163 \text{ for } Q^2 = (80 \text{ GeV})^2,$$

where the Q^2 -dependence is determined by renormalization group equations. For W^{\pm} production the relevant momentum scale is of order M_W . The spin-dependence of the quark densities is rather small, as indicated by the small value of I , so one question that motivates our study is whether the cross-sections for these W^{\pm} -production processes depend significantly on the proton helicity.

In Section II we calculate the cross-section for the process $p_{\lambda}\bar{p} \rightarrow W^{\pm}\gamma$, where $\lambda = L$ or R denotes a left-handed or right-handed proton. This process is sensitive to the $WW\gamma$ anomalous couplings. In Section III we consider the process $p_{\lambda}\bar{p} \rightarrow W^{\pm} W^{\mp}$, which is sensitive to both $WW\gamma$ and WWZ anomalous couplings. The purpose of these calculations is to explore whether polarization of the protons can increase the sensitivity of measurement of anomalous couplings.

2 $W^+\gamma$ production

The Feynman diagrams for the process $p + \bar{p} \rightarrow W^+ + \gamma$ are shown in Figure 2.1. One diagram has a $WW\gamma$ vertex, so the cross-section depends on the anomalous photon coupling parameters $\Delta\kappa_\gamma$ and λ_γ . This process can be used to place limits on the anomalous couplings; calculations of the unpolarized cross-section with anomalous couplings were described in Refs. [9] and [10]. For polarized scattering we expect the cross-section for left-polarized protons to be larger than for right-polarized protons, because the produced W^+ line is always connected to a left-handed quark line. To investigate whether polarizing the proton beam would yield better limits on $\Delta\kappa_\gamma$ and λ_γ , we have calculated the polarized and unpolarized cross-sections. The results of this study are reported in this section.

a. Method of calculation

The cross-section for $p_\lambda + \bar{p} \rightarrow W^+ + \gamma$, where λ is L or R for left-handed or right-handed protons, and with subsequent decay $W^+ \rightarrow \ell^+ + \nu_\ell$, is expressed as

$$\begin{aligned} \sigma(\lambda) = \int_0^1 dx dx' & [\hat{\sigma}_{LR}(xP_1, x'P_2)u_\pm(x)d(x') \\ & + \hat{\sigma}_{LR}(x'P_2, xP_1)\bar{d}_\mp(x)\bar{u}(x')] \end{aligned} \quad (10)$$

where the notation is as follows: The parton cross-section $\hat{\sigma}_{LR}(p_1, p_2)$ is for the process $u_L(p_1) + \bar{d}_R(p_2) \rightarrow W^+ + \gamma$. The upper sign on $u_\pm(x)$ and $\bar{d}_\mp(x)$ is for $\lambda = L$ and the lower sign is for $\lambda = R$. The first line in Eq. (10) corresponds to u, \bar{d} coming from p, \bar{p} , and the second line corresponds to \bar{d}, u coming from p, \bar{p} , respectively. x and x' are the parton momentum fractions in the proton and antiproton respectively. The parton distribution functions are, for example,

$$u_\pm(x) = u \text{ quark with same/opposite helicity as } p$$

$$d(x) = \bar{d} \text{ quark in unpolarized } \bar{p}$$

$\bar{d}_{\mp}(x) = \bar{d}$ quark with opposite/same helicity as p

$\bar{u}(x) = u$ quark in unpolarized \bar{p} .

We also add the contribution for the parton process $c+\bar{s} \rightarrow W^+ + \gamma$, which is, however, small. (We ignore Cabibbo-Kobayashi-Maskawa mixing in this work.) Finally, we add the cross-sections for two lepton decay modes of the W^+ ; that is, ℓ can be either e or μ .

The parton cross-section is calculated from helicity amplitudes for the reaction. In this reaction there is only one nonzero helicity amplitude, with $\lambda_u = L$ and $\lambda_{\bar{d}} = R$, because we approximate the quark masses as 0. In our calculation we calculate the helicity amplitude \mathcal{M}_{LR} numerically. Then the parton cross-section is

$$\hat{\sigma}_{LR} = \int d\Phi |\mathcal{M}_{LR}|^2 \quad (11)$$

where $\int d\Phi$ indicates a phase space integral.

The phase space and x, x' integrations are performed by a Monte-Carlo program, based on the Vegas Monte-Carlo integration routine [11]. The style of the full Monte-Carlo program is the same as the program PAPAGENO [12].

The kinematic cuts we impose on the final ℓ^+ and γ are:

$$\text{rapidity } |\eta_{\ell}| < 3, \quad |\eta_{\gamma}| < 3, \quad (12)$$

$$\text{transverse momentum } p_{T\ell} > 20 \text{ GeV}, \quad p_{T\gamma} > 20 \text{ GeV}, \quad (13)$$

$$\Delta R \equiv \sqrt{(\Delta\eta)^2 + (\Delta\phi)^2} > 0.7, \quad (14)$$

where ΔR is the separation of the ℓ^+ and γ in $\eta - \phi$ space. The only cut on the neutrino is a transverse momentum cut $p_{T\nu} > 20 \text{ GeV}$; that is, we require

$$\cancel{E}_T > 20 \text{ GeV}. \quad (15)$$

At the parton level, there is no background to this process from other interactions, as long as we require the W^+ to decay to leptons. There is an experimental background due to confusion between jets and photons in the detector [10]. However, we do not consider the experimental background here, because our interest is to examine the effect of proton polarization, compared with the unpolarized case.

b. Results

Tables 2.1 and 2.2 show the results of our calculations: the $W^+\gamma$ production cross-section for polarized and unpolarized protons with different values of anomalous couplings $\Delta\kappa_\gamma$ and λ_γ . The cross-section includes the branching ratio $2/9$ for $W^+ \rightarrow \ell^+\nu_\ell$, where the decay modes $\ell = e$ and $\ell = \mu$ are added. (The branching ratio factor $2/9$ is included in all cross-sections reported hereafter.) The cross-section is smallest for $\Delta\kappa_\gamma = 0$ and $\lambda_\gamma = 0$, *i.e.* the Standard Model values. The cross-section depends more strongly on λ_γ than on $\Delta\kappa_\gamma$. Figures 2.2 and 2.3 show plots of the cross-section *vs* $\Delta\kappa_\gamma$ assuming $\lambda_\gamma = 0$, and *vs* λ_γ assuming $\Delta\kappa_\gamma = 0$. As expected, the cross-section is larger for left-handed protons; $\sigma(L)$ is roughly 3 times $\sigma(R)$, and so roughly 1.5 times the unpolarized cross-section. The unpolarized cross-section is by definition equal to $\frac{1}{2}(\sigma(L) + \sigma(R))$.

Figures 2.2 and 2.3 show only the total cross-section (for the cuts specified in Eqs. (12)-(15)). Analysis of differential cross-sections, with respect to relevant kinematic variables, may provide more precise tests of anomalous couplings [10]. For example, Figure 2.4 shows the distribution of $p_{T\gamma}$ for polarized proton scattering, with $\Delta\kappa_\gamma = 0$ (solid line) and $\Delta\kappa_\gamma = -1$ (dashed line). The shapes of the distributions are similar for left- or right-handed protons, but there is an overall difference of magnitude.

c. Limits on $\Delta\kappa_\gamma$ and λ_γ

Tables 2.1 and 2.2 are results from the Monte Carlo calculations of cross-section *vs* anomalous couplings. There is a fairly large effect of proton polarization: $\sigma(L)$ is generally about a factor of 3 larger than $\sigma(R)$. But to see whether an experiment with

polarized protons would yield a significantly better measurement of the anomalous couplings, we must estimate the experimental limit that could be set on $\Delta\kappa_\gamma$ or λ_γ , for a given integrated luminosity.

To estimate the experimental limit that could be placed on an anomalous $WW\gamma$ coupling, we must estimate the uncertainty in an experimental measurement of the cross-section σ . For this analysis we simply assume that the standard deviation in the number of events N is $\delta N = \sqrt{N}$, *i.e.* that N obeys Poisson statistics. (This is an underestimate of the experimental uncertainty; for instance, it does not take into account the experimental background of jets misidentified as photons, *etc.* For our purposes we do not include the efficiency of the detector.) The measured cross-section would be $\sigma = N/L$ where L is the integrated luminosity. The 3-sigma upper limit on σ (*i.e.* 99.7% confidence level) expected from Poisson statistics would be $(N + 3\sqrt{N})/L$. Thus the measurement would rule out a cross-section larger than $\sigma + \delta\sigma_3$, where

$$\delta\sigma_3 = 3\sqrt{\frac{\sigma}{L}} . \tag{16}$$

To estimate the limit that could be placed on $\Delta\kappa_\gamma$ or λ_γ (assuming the anomalous couplings are in fact zero), we compare the uncertainty $\delta\sigma_3$ to the variation of the calculated σ as a function of the anomalous coupling. At the 3-sigma confidence level $\Delta\kappa_\gamma$ would be in the range with

$$|\sigma(\Delta\kappa_\gamma) - \sigma(\Delta\kappa_\gamma = 0)| < \delta\sigma_3 , \tag{17}$$

and similarly for λ_γ .

We assume a Tevatron integrated luminosity equal to 1 fb^{-1} or 10 fb^{-1} . We assume the *same* integrated luminosity for each polarization and for the unpolarized case. Then we obtain the results in Table 2.3, for the experimental limits that could be set on the two anomalous couplings. We emphasize that the numbers in Table

2.3 do not include possible experimental uncertainties; our purpose in estimating the limits that could be placed on $\Delta\kappa_\gamma$ and λ_γ is only to compare the precision from polarized or unpolarized protons.

The left-polarized proton provides a better limit on $\Delta\kappa_\gamma$ or λ_γ , because it has a larger cross-section. The improvement in precision from left-polarized protons, compared to unpolarized, is not very great, because $\sigma(L)$ is only about 1.5 times larger than $\sigma(\text{unpolarized})$, and because the precision on σ is only proportional to $\sigma^{1/2}$. The result is that the total cross-section for left-polarized proton scattering can provide a better limit on $\Delta\kappa_\gamma$ or λ_γ than that for unpolarized scattering, better by about 10 to 20 %.

Another way to consider the effect of proton helicity is to calculate the left-right asymmetry, defined by

$$\mathcal{A} = \frac{\sigma(L) - \sigma(R)}{\sigma(L) + \sigma(R)}. \quad (18)$$

An asymmetry measurement may be accurate experimentally because systematic errors cancel in the ratio. The possible range of \mathcal{A} is $-1 \leq \mathcal{A} \leq 1$, and \mathcal{A} is equal to 0 in a left-right symmetric world. For the *parton* process $q_\lambda \bar{q}' \rightarrow W^+ \gamma$, we have $\mathcal{A} = 1$ because only left-handed quarks contribute. For the *proton* process, the asymmetry is reported in Tables 2.1 and 2.2; we find $\mathcal{A} \approx 0.5$. However, \mathcal{A} depends only weakly on $\Delta\kappa_\gamma$ and λ_γ : \mathcal{A} varies by $\mathcal{O}(10\%)$ over the range of anomalous couplings considered. Thus a measurement of \mathcal{A} to determine $\Delta\kappa_\gamma$ or λ_γ would require high statistics.

We have only considered the process $p_\lambda \bar{p} \rightarrow W^+ \gamma$, and not $W^- \gamma$, because the former is more sensitive to the proton helicity. A W^+ comes from a u quark, whereas a W^- comes from a d quark. The helicity dependence is stronger for u than d in a proton, as seen in Figure 1.1.

3 W^+W^- production

The process $p\bar{p} \rightarrow W^+W^-$ provides a way to test the Standard Model WWV vertices for both $V = \gamma$ and $V = Z^0$. We consider the *doubly* electroweak process

$$p(\lambda) + \bar{p} \rightarrow W^+ (\rightarrow \bar{\ell} + \nu_\ell) + W^- (\rightarrow d + \bar{u}) , \quad (19)$$

and also the process in which the W^- decays leptonically while the W^+ decays to 2 jets. The complete set of Feynman diagrams with the final state $\bar{\ell}\nu d\bar{u}$ includes diagrams that do not have the form of W^+W^- production. Figure 3.1 shows the complete set of Feynman diagrams for the parton process

$$u + \bar{u} \rightarrow W^+ + d + \bar{u} , \quad \text{with } W^+ \rightarrow \bar{\ell} + \nu_\ell ; \quad (20)$$

there is similarly a set of diagrams for the process

$$d + \bar{d} \rightarrow W^+ + d + \bar{u} , \quad \text{with } W^+ \rightarrow \bar{\ell} + \nu_\ell . \quad (21)$$

Also, there are similar diagrams for production of $W^- + u + \bar{d}$, with $W^- \rightarrow \ell + \bar{\nu}_\ell$. (The complete set of diagrams for the final state $\bar{\ell}\nu d\bar{u}$, or $\ell\bar{\nu}u\bar{d}$, includes additional diagrams in which the leptons are not decay products of a single narrow W^\pm .) These parton processes involve the $WW\gamma$ and WWZ vertices in some Feynman diagrams, so the cross-sections depend on anomalous WWV couplings, *i.e.* the parameters $\Delta\kappa_\gamma, \Delta\kappa_Z, \lambda_\gamma, \lambda_Z$. In this section we study the cross-section as a function of these non-Standard parameters, for polarized protons. The purpose is again to see whether an experiment with a polarized proton beam would yield a stronger test of the electroweak triple-boson vertices.

Some, though not all, of the Feynman diagrams in Fig. 3.1 have the form of W^+W^- production, followed by decays of the W 's, one leptonically and the other into two jets. At 2 TeV center-of-mass energy, the cross-section is dominated by the W^+W^-

production. Therefore, as explained further below, we approximate the cross-section by W^+W^- production. The cross-sections for $\ell\bar{\nu}u\bar{d}$ and $\bar{\ell}\nu\bar{u}d$ final states are equal in this approximation, because either W is equally likely to decay leptonically.

A related process is $W^\pm Z^0$ production, where the Z^0 decays to 2 jets, *e.g.*,

$$u + \bar{d} \rightarrow W^+ \left(\rightarrow \ell^+ + \nu_\ell \right) + Z^0 \left(\rightarrow q + \bar{q} \right) . \quad (22)$$

In our calculations we ignore the $W^\pm Z^0$ production. In a theoretical calculation the W^+W^- production is distinguishable from the $W^\pm Z^0$ production. However, in an experiment these two processes are tangled together, because they are both observed as $W^\pm + 2 \text{ jets}$. In our W^+W^- calculation we impose a kinematic cut on the invariant mass M_{2j} of the 2 jets, making M_{2j} approximately equal to the W^\pm mass; specifically we take M_{2j} between 70 and 90 GeV. (This cut reduces the QCD background of $W^\pm + 2 \text{ jets}$.) But even with this cut on M_{2j} there would still be an overlap between W^+W^- production and $W^\pm Z^0$ production. The purpose of our calculation is a theoretical study of the effect of proton polarization on the cross-section. A complete analysis of experimental data would need to include both the W^+W^- and $W^\pm Z^0$ processes together.

The method of calculation is similar to Sec. 2, but with some differences. In Sec. 2 only one parton helicity combination contributes, $u(L)\bar{d}(R)$. Here two helicity combinations contribute, for example $u(L)\bar{u}(R)$ and $u(R)\bar{u}(L)$, and we include both. In fact, for Standard couplings the contribution from $u(R)\bar{u}(L)$ is very small compared to $u(L)\bar{u}(R)$, because of interference between Feynman diagrams, so the parton-level process still depends strongly on quark helicities. A more important difference is that in Sec. II there was no parton-level background process, whereas here we have a large background from electroweak+QCD processes.

a. Background, Approximations, and Cuts

The parton-level background to this process is the production of $W^\pm + 2 \text{ jets}$ by processes with one electroweak vertex and one QCD vertex. These processes do not interfere quantum mechanically with our doubly electroweak signal process, because they have a different color structure; for example, the $q\bar{q}g$ vertex is color octet, where g denotes the gluon, whereas $q\bar{q}\gamma$ or $q\bar{q}Z^0$ vertices are color singlet. However the final states are indistinguishable experimentally, so the doubly electroweak reaction is hidden in a background of electroweak-QCD reactions.

We have calculated the background cross-section from the helicity amplitudes for a complete set of $W^\pm + 2 \text{ jets}$ processes [13], with the polarized parton distribution functions described in Sec. 1. The background reactions should depend strongly on the helicity of the proton: The produced W^\pm must connect to a left-handed quark or right-handed antiquark for massless quarks, by the V–A coupling; the density of quarks of given helicity depends on the helicity of the proton. By contrast, for the signal reaction the diagrams *with anomalous $WW\gamma$ or WWZ vertices* do not require any specific helicities of the incoming quarks. Thus the signal reaction will have a different dependence on proton helicity than the background. The important question is whether the signal-to-background ratio in the measurement of anomalous WWV couplings is better for left- or right-polarized protons.

To reduce the background we impose a cut on the invariant mass M_{2j} of the 2 jets, putting M_{2j} approximately equal to M_W . The solid curve in Figure 3.2 shows the distribution of the invariant mass of the two jets produced by the complete doubly electroweak process with final state $q\bar{q}'W^+$, with $W^+ \rightarrow \bar{\ell}\nu_\ell$, for $\sqrt{s} = 2 \text{ TeV}$. The $q\bar{q}'$ invariant mass is peaked at the W^+ mass. Because the cross-section is dominated by the W^+ resonance, we approximate the calculation by keeping only the Feynman diagrams that produce a W^+W^- pair, which is an accurate simplifying approximation. Furthermore, we *require* the $q\bar{q}'$ invariant mass to be approximately equal to the W^\pm mass: we calculate the cross-section only for events with $M_{q\bar{q}'}$ between 70 and 90 GeV. The dotted curve in Figure 3.2 shows the 2-jet mass distribution when we

neglect all but the W^+W^- pair production diagrams and also require the 2-jet mass to be between 70 and 90 GeV. With this M_{2j} cut, the complete doubly electroweak process is practically the same as production of W^+W^- followed by leptonic decay of W^\pm and quark-antiquark decay of W^\mp . For comparison, Figure 3.3 shows the 2-jet mass distribution of the background processes with the kinematic cuts listed in Eqs. (23)-(26) below; the cut $70 \text{ GeV} < M_{q\bar{q}'} < 90 \text{ GeV}$ reduces the total background significantly, because there is no resonant effect in the background processes.

In addition to the M_{2j} -cut just described, we impose the following kinematic cuts on all the final-state particles except the neutrino:

$$\text{rapidity } |\eta| < 3, \tag{23}$$

$$\text{transverse momentum } p_T > 15 \text{ GeV}, \tag{24}$$

$$\Delta R \equiv \sqrt{(\Delta\eta)^2 + (\Delta\phi)^2} > 0.7, \tag{25}$$

where ΔR is the separation of any pair of final particles not including the neutrino. In the case of the neutrino, we impose only a transverse momentum cut, $p_{T\nu} > 15 \text{ GeV}$; *i.e.*,

$$\cancel{E}_T > 15 \text{ GeV}. \tag{26}$$

Figure 3.4 is another comparison between the complete doubly electroweak calculation, shown as the solid line, and the simplified approximation (W^+W^- production with subsequent W^\pm decays), shown as the dashed line. Figure 3.4 compares the $\sqrt{\hat{s}}$ distributions, where $\sqrt{\hat{s}}$ is the center of mass energy of the parton-level process. Again, the two calculations are practically equal.

We also consider, separately, a cut requiring large $\sqrt{\hat{s}}$, specifically $\sqrt{\hat{s}} > 340 \text{ GeV}$. The variable $\sqrt{\hat{s}}$ is important because the effect of anomalous coupling increases with

$\sqrt{\hat{s}}$. Figure 3.5 compares signal and background as a function of $\sqrt{\hat{s}}$. This figure shows why large- $\sqrt{\hat{s}}$ is interesting: the signal-to-background ratio is larger, and the dependence on $\Delta\kappa$ and λ is stronger, for large $\sqrt{\hat{s}}$. Figure 3.6 compares signal and background for $\sqrt{\hat{s}} > 340$ GeV. On the other hand, this energy cut reduces drastically the total number of events, so it becomes a question of detailed calculation to see whether it is a real advantage, given the available luminosity. Our calculation is for $\sqrt{s} = 2$ TeV. A $p\bar{p}$ collider with higher center-of-mass energy would produce more events in the interesting region of phase space with large $\sqrt{\hat{s}}$, and provide stronger tests of the anomalous WWV couplings.

It is difficult to determine $\sqrt{\hat{s}}$ accurately in an experimental event, because that requires measurement of jet momenta and missing neutrino momentum. The z -component of the neutrino momentum $p_{\nu z}$ can be obtained up to a two-fold ambiguity by solving the mass constraint for the W -boson, $M_W^2 = (p_\ell + p_\nu)^2$. One way to choose $p_{\nu z}$ is to select the solution with smaller absolute value, because a hard scattering process tends to produce final products in the central rapidity region with large transverse momenta. Given $p_{\nu z}$ it is straightforward to calculate $\sqrt{\hat{s}}$ from the 4-momenta of ℓ, ν , and the 2 jets. Alternatively, another way to select large $\sqrt{\hat{s}}$ is to require large transverse mass of the final state of the hard scattering process [14]; however, we have not pursued that approach in this work.

b. Results

For the cross-section calculations that follow, we set $Q = \sqrt{\hat{s}}$, where Q is the momentum scale used in the parton distribution functions. The uncertainties we quote are only the statistical Monte-Carlo uncertainties. The theoretical uncertainty due the choice of Q scale is discussed briefly later. The cross-section includes the branching ratio $2/9$ for leptonic decay of one W (into either electron or muon plus neutrino). The cross-section also includes the branching ratio $6/9$ for 2-jet decay of the other W , *e.g.* $W^+ \rightarrow u\bar{d}$ and $W^+ \rightarrow c\bar{s}$. (Again we ignore CKM mixing.) The overall branching ratio $(2/9) \times (6/9) = 4/27$ is always included in the cross-sections

reported hereafter for W^+W^- production. Note that we consider separately the rates for $\ell^+ + jets$ and $\ell^- + jets$.

Figures 3.7 to 3.9 show the results as plots of signal cross-section *vs* anomalous coupling parameters. Since our signal process involves the creation of a W^+W^- pair with subsequent decays of the W^+ and W^- , the signal cross-section is the same regardless of which W decays to leptons, in the narrow-width approximation. We need to compare the signal cross-section to the QCD background cross-section. We may consider the background for either W^+ or W^- production, and then choose the W charge that has the smaller background cross-section. For *polarized* protons, the background cross-sections for W^+ or W^- production are different. For instance, for a left-handed proton the background process $p(L) + \bar{p} \rightarrow W^+ + 2 jets$ has a larger rate than $p(L) + \bar{p} \rightarrow W^- + 2 jets$, because the probability of finding $u(L)$ (which produces W^+) inside $p(L)$ is larger than $d(L)$ (which produces W^-), as implied by Fig. 1.1; $u(R)$ and $d(R)$ do not contribute to the constituent cross-section of the $W^\pm + 2 jets$ background process because the weak charged current is left-handed. Therefore it is advantageous experimentally to observe the $W^-(\rightarrow \ell\bar{\nu}) + 2 jets$ mode for a left-polarized proton beam, and similarly the $W^+(\rightarrow \bar{\ell}\nu) + 2 jets$ for a right-polarized proton beam. (For *unpolarized* scattering the production rates of W^+ and W^- are equal by CP invariance; but for scattering of polarized protons on unpolarized antiprotons, CP invariance does not apply.) Since the signal process is symmetric with respect to the charge of the W that decays leptonically, the process with the smaller background has a better signal-to-background ratio. Hereafter we apply this strategy when comparing signal and background rates in the Tables.

The program we have used to calculate the electroweak+QCD background, which comes from many processes [13], is set up to calculate the cross-section for production of $W^- + 2 jets$. To find the cross-section for production of $W^+ + 2 jets$, we calculate the rate for W^- production with polarized *anti-protons*, which is equal to the rate we

want by CP invariance:

$$\sigma(p + \bar{p}(L) \rightarrow W^- + 2 \text{ jets}) = \sigma(p(R) + \bar{p} \rightarrow W^+ + 2 \text{ jets}) \quad (27)$$

$$\sigma(p + \bar{p}(R) \rightarrow W^- + 2 \text{ jets}) = \sigma(p(L) + \bar{p} \rightarrow W^+ + 2 \text{ jets}) \quad (28)$$

Tables 3.1 to 3.5 give the calculated cross-sections. Table 3.5 lists the background cross-sections for different proton helicities. As expected, $\sigma(L)$ is larger than $\sigma(R)$ for W^+ production: the W^+ must come from a $u(L)$, and the density of $u(L)$ is larger in $p(L)$ than in $p(R)$. On the other hand, $\sigma(L)$ is *smaller* than $\sigma(R)$ for W^- production: the W^- must come from a $d(L)$, and the density of $d(L)$ is *smaller* in $p(L)$ than in $p(R)$, because $\Delta d(x)$ is mostly negative, as shown in Fig. 1.1.

Table 3.5 lists cross-sections calculated using the polarized parton distribution functions of Sec. 1, and also, for comparison, unpolarized cross-sections calculated using CTEQ2 parton distribution functions [15]. We have used the leading-order set CTEQ2L for our studies. The CTEQ2 results are consistent with the average of the two proton helicities, within the uncertainty of the Monte Carlo calculations.

c. Limits on $\Delta\kappa_\gamma$, $\Delta\kappa_Z$, λ_γ , and λ_Z

We estimate limits on anomalous couplings that could be set by experiments at $\sqrt{s} = 2$ TeV. Since there is a large background for this process, the limits depend on the background cross-section σ_B . Again, as in our analysis of the $W^+\gamma$ process, we assume that in an experiment with N events the standard deviation of N is $\delta N = \sqrt{N}$. At the three-sigma confidence level, the uncertainty of σ is

$$\delta\sigma_3 = 3\sqrt{\frac{\sigma}{L}}, \quad (29)$$

which is the same as Eq. (16), except that here σ is the sum of signal and background cross-sections. We consider integrated luminosity $L = 1 \text{ fb}^{-1}$ and $L = 10 \text{ fb}^{-1}$.

To calculate the limit that could be set on an anomalous coupling parameter, *e.g.* $\Delta\kappa_\gamma$, assuming the actual value of the parameter is zero, we compare the statistical uncertainty $\delta\sigma_3$ to the variation of the calculated cross-section as a function of $\Delta\kappa_\gamma$. At the three-sigma confidence level, $\Delta\kappa_\gamma$ is in the range with

$$|\sigma(\Delta\kappa_\gamma) - \sigma(\Delta\kappa_\gamma = 0)| < \delta\sigma_3 . \quad (30)$$

For example, Figure 3.7c shows σ *vs* $\Delta\kappa$ for unpolarized scattering. Three possibilities are shown: (i) the effect of $\Delta\kappa_\gamma$ with $\Delta\kappa_Z = 0$, (ii) the effect of $\Delta\kappa_Z$ with $\Delta\kappa_\gamma = 0$, and (iii) the effect if $\Delta\kappa_\gamma = \Delta\kappa_Z$. The background cross-section is given in Table 3.5. Then Tables 3.6 and 3.7 list the limits that could be set on $\Delta\kappa$ (and also λ) for these three cases. The estimated limits in Table 3.6 are from events with arbitrary $\sqrt{\hat{s}}$, and the limits in Table 3.7 are from events with $\sqrt{\hat{s}} > 340$ GeV.

Our purpose is to determine whether measurement of the cross-section with polarized protons leads to stronger limits on anomalous couplings than with unpolarized protons. Tables 3.6 and 3.7 show that the limit is stronger with left-polarized protons, assuming the same integrated luminosity as for unpolarized scattering. The constraints on either $\Delta\kappa_\gamma$ or λ_γ alone from the W^+W^- channel are not as strong as those obtained from studying the $W^+\gamma$ channel. The constraints on $\Delta\kappa_Z$ and λ_Z are about a factor of 2 better than those on $\Delta\kappa_\gamma$ and λ_γ from the W^+W^- channel. For models with a linear SU(2) symmetry, such that $\kappa_\gamma = \kappa_Z$ and $\lambda_\gamma = \lambda_Z$, the constraint on $\Delta\kappa_\gamma$ is about a factor of 2 better than from the $W^+\gamma$ channel, while the constraint on λ_γ is about the same as from the $W^+\gamma$ channel, after selecting the large $\sqrt{\hat{s}}$ region. In general, selecting large $\sqrt{\hat{s}}$ (> 340 GeV) improves the significance of signal to background by about a factor of 2.

d. Interpretation of the results

The limits described above show how this process, W^+W^- production with polarized protons, tests the WWV vertex. The estimated limits on anomalous couplings include only simple statistical uncertainty, based on Poisson statistics ($\delta N = \sqrt{N}$);

they do not include experimental uncertainty due to detector inefficiency or theoretical uncertainty of parton distribution functions or Q scale.

For example, the background calculation depends on the choice of parton momentum scale Q . Table 3.8 shows how the background cross-section, for unpolarized scattering, depends on the choice of Q . We used $Q = \sqrt{\hat{s}}$ in our calculations. $Q = 2M_W$ or $Q = \sqrt{\hat{s}}/2$ would also be reasonable choices. The cross-sections for the three choices differ by about 20%. This theoretical uncertainty due to dependence on scale choice is larger than the statistical uncertainty analysed above. It is thus difficult to extract the signal cross-section unless the uncertainty in the background cross-section is reduced, by including higher-order QCD effects to reduce the dependence on Q scale. On the other hand, given large luminosity the details of the QCD background processes, *e.g.* the shapes of $\sqrt{\hat{s}}$ distributions, can be measured directly from data to discriminate between different theoretical predictions from different scale choices. Therefore we anticipate that background rates will eventually be better known, and allow us to extract signal rates.

Our purpose in this work is to study the effect of proton polarization. For this study we have analysed only the *total cross-section* as a function of $\Delta\kappa$ and λ . Stronger constraints on $\Delta\kappa$ and λ may be set by analysing differential cross-sections, with respect to variables for which the distribution of events is sensitive to $\Delta\kappa$ or λ [9, 10]. It would be interesting to find kinematic variables *dependent on proton helicity* for which the distribution of events is sensitive to $\Delta\kappa$ or λ , to further test the triple-boson couplings with polarized proton scattering.

4 Discussion and Conclusions

We have studied the potential of a polarized proton beam at the Tevatron collider for measuring the tri-boson couplings $WW\gamma$ and WWZ . Because the polarized parton distribution functions in the relevant kinematic region (*i.e.*, x -values) are not yet precise enough to give definite detailed predictions about the rates of the signal and the backgrounds, we have concentrated on the comparisons between the total event rates from a polarized- and an unpolarized- proton beam. As summarized in Tables 2.3, 3.6 and 3.7, we found that with a polarized proton beam the limits on non-standard parameters $\Delta\kappa_\gamma$, λ_γ , $\Delta\kappa_Z$ and λ_Z are somewhat improved compared to those obtained from an unpolarized proton beam. We anticipate that these results can be further improved by studying detailed distributions of relevant kinematic variables. Generally a factor of 2 improvement in measuring these non-standard parameters is expected, after selecting kinematic regions where the signal becomes more important, as illustrated in Tables 3.6 and 3.7.

Reliable predictions of distributions of kinematic variables will require more precise polarized parton distribution functions. Measurements of polarized proton-antiproton reactions, such as single- W^\pm production with a polarized proton beam, will yield new information on spin-dependent parton distributions. Thus the use of polarized scattering to test fundamental physics, and the determination of the spin structure of the proton, would proceed together.

One interesting feature that we found about the polarized collider program is that it is possible to select the polarization state of the proton beam to enhance the ratio of signal to background for a specific charge mode of the final state. This was demonstrated in studying the process $p\bar{p} \rightarrow W^+W^- \rightarrow \ell^\pm \bar{\nu}_\ell + 2 \text{ jets}$. For the final state with a positive charged lepton (ℓ^+), one can select the polarization of the proton beam to be right-handed to improve the signal-to-background ratio because the QCD background process $p(R)\bar{p} \rightarrow W^+(\rightarrow \ell^+\nu_\ell) + 2 \text{ jets}$ has a smaller rate than

$p(L)\bar{p} \rightarrow W^+(\rightarrow \ell^+\nu_\ell) + 2 \text{ jets}$. The signal rate, in contrast, is independent of the charge mode of the isolated lepton from the W -boson decay because either W^+ or W^- can decay into the charged lepton. We expect that similar tricks can be applied to other polarized physics measurements, such as the *lepton + jet* mode of the $t\bar{t}$ pair production from $q\bar{q}$ and gg fusion processes.

Acknowledgements

We thank Ray Brock and Harry Weerts for discussions on polarized proton scattering. We especially thank Glenn Ladinsky for providing us with his program to calculate polarized parton distribution functions. The work of C.-P. Y. was supported by NSF grant No. PHY-9309902.

References

- [1] *Acceleration of Polarized Protons to 120 and 150 GeV in the Fermilab Main Injector*, University of Michigan Report UM HE 92-5, March 1992 (unpublished); *Progress Report: Acceleration of Polarized Protons to 1 TeV in the Fermilab Tevatron*, University of Michigan Report UM HE 94-15, August 1994 (unpublished).
- [2] Expression of Interest, *Polarization Physics at the Tevatron Collider*, by R. Brock, G. A. Ladinsky, D. Stump, M. Wiest, H. Weerts, C.-P. Yuan, and G. Blazey, May-5, 1994.
- [3] T. D. Lee and C. N. Yang, Phys. Rev. **128**, 885 (1962).
- [4] H. Georgi, Nucl. Phys. **B361**, 339 (1991). H. Georgi, *Weak Interactions and Modern Particle Theory* (The Benjamin/Cummings Publishing Company, 1984).
- [5] Morfin and W. K. Tung, Z. Phys. **C52**, 13 (1991).
- [6] G. A. Ladinsky, Phys. Rev. **D46**, 3789 (1992); **D47**, 3086 (1993).
- [7] P. L. Anthony *et al.*, Phys. Rev. Lett. **71**,959 (1993); J. Ashman *et al.*, Nucl. Phys. **B328**,1 (1989); B. Adeva, *et al.*, Phys. Lett. **B302**, 533 (1993).
- [8] Spin Muon Collaboration, Phys. Lett. **B329**, 399 (1994).
- [9] U. Baur and E. Berger, Phys. Rev. **D41**, 1476 (1990).
- [10] U. Baur, T. Han, and J. Ohnemus, Phys. Rev. **D48**, 5140 (1993).
- [11] G. P. LePage, J. Comp. Phys. **27**, 192 (1978).
- [12] I. Hinchliffe, LBL Theoretical Physics Group.
- [13] K. Hagiwara and D. Zeppenfeld, Nucl. Phys. **B313**, 560 (1989). Our program is based on a program by D. Zeppenfeld, W. Long, T. Han, and D. Zeppenfeld. We

have modified their code to select helicity amplitudes for specific helicity states of the initial partons, and to use polarized parton distribution functions.

- [14] J. Bagger, V. Barger, K. Cheung, J. Gunion, T. Han, G. Ladinsky, R. Rosenfeld, and C.-P. Yuan, *Rhys. Rev.* **D49**, 1246 (1994).
- [15] J. Botts, J. Huston, H. L. Lai, J. G. Morfin, J. F. Owens, J. Qiu, W.-K. Tung, H. Weerts, Michigan State Univeristy preprint MSUTH-93/17 (unpublished).

Tables

Table 2.1. Cross-section for the process $p\bar{p} \rightarrow W^+\gamma$ with polarized protons, for different values of the anomalous coupling $\Delta\kappa_\gamma$, assuming $\lambda_\gamma = 0$. Cross-sections are in pb. The branching ratio $2/9$ for $W^+ \rightarrow e^+\nu_e$ or $\mu^+\nu_\mu$ is included. The unpolarized case was calculated separately using CTEQ2 parton distribution functions, for comparison. The asymmetry \mathcal{A} , defined in Eq. (18), is calculated by fitting the data to a parabola.

$p\lambda\bar{p} \rightarrow W^+\gamma$ cross-sections in pb				
$\Delta\kappa_\gamma$	p(R)	p(L)	Unpol	\mathcal{A}
2.0	0.49 ± 0.01	1.44 ± 0.01	0.98 ± 0.01	0.514
1.5	0.39 ± 0.01	1.08 ± 0.01	0.75 ± 0.01	0.504
1.0	0.29 ± 0.01	0.86 ± 0.01	0.59 ± 0.01	0.491
0.5	0.25 ± 0.01	0.72 ± 0.01	0.51 ± 0.01	0.480
0.0	0.25 ± 0.01	0.69 ± 0.01	0.47 ± 0.01	0.475
-0.5	0.27 ± 0.01	0.75 ± 0.01	0.54 ± 0.01	0.480
-1.0	0.32 ± 0.01	0.94 ± 0.01	0.63 ± 0.01	0.491
-1.5	0.41 ± 0.01	1.23 ± 0.01	0.83 ± 0.01	0.504
-2.0	0.53 ± 0.02	1.57 ± 0.02	1.09 ± 0.02	0.514

Table 2.2. Cross-section for the process $p\bar{p} \rightarrow W^+\gamma$ with polarized protons, for different values of the anomalous coupling λ_γ , assuming $\Delta\kappa_\gamma = 0$. Cross-sections are in pb. The unpolarized case was calculated separately using CTEQ2 parton distribution functions, for comparison. The asymmetry \mathcal{A} , defined in Eq. (18), is calculated by fitting the data to a parabola.

$p\lambda\bar{p} \rightarrow W^+\gamma$ cross-sections in pb.				
λ_γ	p(R)	p(L)	Unpol	\mathcal{A}
2.0	1.73 ± 0.03	7.47 ± 0.03	4.55 ± 0.03	0.613
1.5	1.11 ± 0.02	4.47 ± 0.02	2.72 ± 0.02	0.602
1.0	0.62 ± 0.01	2.32 ± 0.01	1.50 ± 0.01	0.580
0.5	0.35 ± 0.03	1.14 ± 0.03	0.75 ± 0.03	0.530
0.0	0.24 ± 0.01	0.68 ± 0.01	0.49 ± 0.01	0.478
-0.5	0.34 ± 0.01	1.05 ± 0.01	0.71 ± 0.01	0.530
-1.0	0.57 ± 0.01	2.19 ± 0.01	1.39 ± 0.01	0.580
-1.5	0.99 ± 0.03	4.13 ± 0.03	2.59 ± 0.03	0.602
-2.0	1.64 ± 0.03	6.87 ± 0.03	4.16 ± 0.03	0.613

Table 2.3. Limits on non-Standard couplings, from $p\bar{p} \rightarrow W^+\gamma$ with polarized and unpolarized protons. The upper number is for 1 fb^{-1} integrated luminosity, and the lower number (in parentheses) is for 10 fb^{-1} .

Parameter	Limits		
	$p(R)$	$p(L)$	Unpol
$\Delta\kappa_\gamma$	± 0.89 (± 0.50)	± 0.62 (± 0.35)	± 0.70 (± 0.39)
λ_γ	± 0.36 (± 0.20)	± 0.22 (± 0.13)	± 0.26 (± 0.14)

Table 3.1. Purely electroweak cross-sections, in pb, for $p(R)\bar{p} \rightarrow W^+ + 2 \text{ jets}$, with $W^+ \rightarrow \bar{\ell}\nu$ where $\ell = e$ or μ ; the proton is right-handed. The cross-section for $p(R)\bar{p} \rightarrow W^- + 2 \text{ jets}$ is the same. The branching ratio $(2/9) \times (6/9) = 4/27$ is included.

<i>Electroweak cross-sections in pb; right-polarized proton.</i>						
Value	Varied quantity					
	$\Delta\kappa_\gamma$	$\Delta\kappa_Z$	$\Delta\kappa_\gamma = \Delta\kappa_Z$	λ_γ	λ_Z	$\lambda_\gamma = \lambda_Z$
1.00	0.604±.012	1.120±.020	1.064±.020	0.740±.020	1.344±.028	1.444±.032
0.75	0.534±.012	0.774±.016	0.816±.016	0.602±.014	0.952±.018	1.004±.020
0.50	0.496±.012	0.600±.012	0.588±.012	0.524±.012	0.688±.016	0.712±.016
0.25	0.456±.012	0.484±.012	0.484±.012	0.472±.012	0.520±.012	0.520±.012
0.00	0.456±.012	0.456±.012	0.456±.012	0.456±.012	0.456±.012	0.456±.012
-0.25	0.484±.012	0.508±.012	0.516±.012	0.480±.012	0.504±.012	0.516±.012
-0.50	0.540±.012	0.628±.012	0.676±.012	0.548±.012	0.664±.016	0.708±.016
-0.75	0.620±.012	0.822±.014	0.908±.016	0.642±.016	0.920±.018	1.000±.020
-1.00	0.716±.016	1.172±.024	1.356±.028	0.768±.016	1.288±.024	1.444±.028

Table 3.2. Purely electroweak cross-sections, in pb, for $p(L)\bar{p} \rightarrow W^+ + 2 \text{ jets}$, with $W^+ \rightarrow \bar{\ell}\nu$ where $\ell = e$ or μ ; the proton is left-handed. The cross-section for $p(L)\bar{p} \rightarrow W^- + 2 \text{ jets}$ is the same. The branching ratio $(2/9) \times (6/9) = 4/27$ is included.

<i>Electroweak cross-sections in pb; left-polarized proton.</i>						
Value	Varied quantity					
	$\Delta\kappa_\gamma$	$\Delta\kappa_Z$	$\Delta\kappa_\gamma = \Delta\kappa_Z$	λ_γ	λ_Z	$\lambda_\gamma = \lambda_Z$
1.00	1.08±.02	1.88±.04	2.68±.08	1.26±.04	2.60±.04	3.84±.08
0.75	1.02±.02	1.48±.04	1.92±.04	1.10±.02	1.84±.04	2.60±.08
0.50	0.98±.02	1.16±.02	1.34±.04	1.04±.02	1.38±.04	1.72±.08
0.25	0.98±.02	1.00±.02	1.02±.02	0.98±.02	1.06±.02	1.16±.02
0.00	0.96±.02	0.96±.02	0.96±.02	0.94±.02	0.94±.02	0.98±.02
-0.25	0.98±.02	1.08±.02	1.16±.04	1.00±.02	1.06±.02	1.16±.04
-0.50	1.04±.02	1.32±.02	1.58±.04	1.04±.02	1.40±.04	1.72±.04
-0.75	1.14±.02	1.72±.04	2.28±.04	1.14±.02	1.86±.04	2.60±.08
-1.00	1.24±.04	2.24±.04	3.20±.08	1.26±.04	2.56±.04	3.88±.08

Table 3.3. Purely electroweak cross-sections, in pb, for $p\bar{p} \rightarrow W^+ + 2 \text{ jets}$, with $W^+ \rightarrow \bar{\ell}\nu$ where $\ell = e$ or μ ; the proton is unpolarized. The cross-section for $p\bar{p} \rightarrow W^- + 2 \text{ jets}$ is the same. The branching ratio $(2/9) \times (6/9) = 4/27$ is included. These values were calculated independently using the Morfin-Tung ppdf's; the cross-section for unpolarized protons is equal to the average of cross-section for left and right polarized protons.

<i>Electroweak cross-sections in pb; unpolarized proton</i>						
Value	Varied quantity					
	$\Delta\kappa_\gamma$	$\Delta\kappa_Z$	$\Delta\kappa_\gamma = \Delta\kappa_Z$	λ_γ	λ_Z	$\lambda_\gamma = \lambda_Z$
1.00	$0.84\pm.02$	$1.50\pm.04$	$1.88\pm.06$	$1.00\pm.02$	$1.98\pm.06$	$2.64\pm.06$
0.75	$0.78\pm.02$	$1.14\pm.02$	$1.36\pm.02$	$0.86\pm.02$	$1.40\pm.04$	$1.80\pm.06$
0.50	$0.74\pm.02$	$0.88\pm.02$	$0.96\pm.02$	$0.78\pm.02$	$1.04\pm.02$	$1.22\pm.02$
0.25	$0.72\pm.02$	$0.74\pm.02$	$0.76\pm.02$	$0.72\pm.02$	$0.80\pm.02$	$0.84\pm.02$
0.00	$0.72\pm.02$	$0.72\pm.02$	$0.72\pm.02$	$0.70\pm.02$	$0.70\pm.02$	$0.70\pm.02$
-0.25	$0.72\pm.02$	$0.80\pm.02$	$0.84\pm.02$	$0.74\pm.02$	$0.86\pm.02$	$0.84\pm.02$
-0.50	$0.78\pm.02$	$0.98\pm.02$	$1.14\pm.02$	$0.80\pm.02$	$1.04\pm.02$	$1.22\pm.02$
-0.75	$0.88\pm.02$	$1.28\pm.02$	$1.60\pm.02$	$0.88\pm.02$	$1.38\pm.04$	$1.80\pm.06$
-1.00	$0.98\pm.02$	$1.70\pm.04$	$2.28\pm.06$	$1.02\pm.02$	$1.92\pm.04$	$2.66\pm.06$

Table 3.4. Electroweak cross-sections, in pb, for W^+W^- production with non-Standard couplings, with polarized or unpolarized protons, and with a large- $\sqrt{\hat{s}}$ cut, $\sqrt{\hat{s}} > 340$ GeV. One W decays leptonically, the other to 2 jets, and the branching ratio 4/27 is included in the cross-section. Two assumptions on non-Standard couplings are listed: $\Delta\kappa_\gamma = \Delta\kappa_Z$ with $\lambda_\gamma = \lambda_Z = 0$, and $\lambda_\gamma = \lambda_Z$ with $\Delta\kappa_\gamma = \Delta\kappa_Z = 0$.

<i>Electroweak cross-sections in pb, with $\sqrt{\hat{s}} > 340$ GeV</i>						
Value	Varied parameter					
	$\Delta\kappa_\gamma = \Delta\kappa_Z$			$\lambda_\gamma = \lambda_Z$		
	$p(L)$	$p(R)$	Unpol	$p(L)$	$p(R)$	Unpol
0.75	0.720±.016	0.208±.004	0.456±.012	1.196±.028	0.316±.008	0.756±.012
0.50	0.380±.008	0.110±.002	0.236±.004	0.592±.012	0.162±.004	0.368±.008
0.25	0.180±.004	0.052±.002	0.112±.002	0.248±.008	0.070±.002	0.152±.004
0.00	0.132±.004	0.038±.002	0.082±.002	0.132±.004	0.038±.000	0.082±.002
-0.25	0.228±.004	0.066±.002	0.142±.004	0.244±.008	0.070±.002	0.156±.004
-0.50	0.484±.012	0.138±.002	0.304±.008	0.604±.016	0.166±.004	0.376±.008
-0.75	0.876±.016	0.244±.004	0.556±.012	1.160±.028	0.316±.008	0.732±.016

Table 3.5. QCD background cross-sections for $p\bar{p} \rightarrow W^\pm + 2 \text{ jets}$, for various proton polarizations and kinematic cuts. The unpolarized cases $\sigma(p\bar{p} \rightarrow W^+ 2j) = \sigma(p\bar{p} \rightarrow W^- 2j)$ were calculated separately using CTEQ2 parton distribution functions.

<i>W+2 jet Background</i>	
process	σ (pb)
<i>without 2 jet mass cut:</i>	
$p(R)\bar{p} \rightarrow W^- 2j$	$50.56 \pm .58$
$p(L)\bar{p} \rightarrow W^- 2j$	$41.36 \pm .52$
$p(L)\bar{p} \rightarrow W^+ 2j$	$65.46 \pm .78$
$p(R)\bar{p} \rightarrow W^+ 2j$	$26.84 \pm .28$
$p\bar{p} \rightarrow W^+ 2j$	$45.30 \pm .50$
<i>with 2 jet mass cut (70-90 GeV):</i>	
$p(R)\bar{p} \rightarrow W^- 2j$	$7.324 \pm .070$
$p(L)\bar{p} \rightarrow W^- 2j$	$5.910 \pm .056$
$p(L)\bar{p} \rightarrow W^+ 2j$	$9.404 \pm .092$
$p(R)\bar{p} \rightarrow W^+ 2j$	$3.874 \pm .034$
$p\bar{p} \rightarrow W^+ 2j$	$6.514 \pm .060$
<i>with 2 jet mass cut</i>	
<i>and $\sqrt{\hat{s}} > 340$ GeV:</i>	
$p(R)\bar{p} \rightarrow W^- 2j$	$0.348 \pm .004$
$p(L)\bar{p} \rightarrow W^- 2j$	$0.308 \pm .004$
$p(L)\bar{p} \rightarrow W^+ 2j$	$0.520 \pm .004$
$p(R)\bar{p} \rightarrow W^+ 2j$	$0.144 \pm .004$
$p\bar{p} \rightarrow W^+ 2j$	$0.358 \pm .002$

Table 3.6. Limits on anomalous couplings that could be set from $p\bar{p} \rightarrow W^\pm + 2 \text{ jets}$ with polarized or unpolarized protons. The numbers in parentheses are for 10 fb^{-1} integrated luminosity, and the other numbers are for 1 fb^{-1} integrated luminosity.

Parameter	Limits		
	$p(R)$	$p(L)$	Unpol
$\Delta\kappa_\gamma$	± 0.89	± 1.10	± 1.06
$\Delta\kappa_Z$	± 0.56	± 0.47	± 0.54
$\Delta\kappa_\gamma = \Delta\kappa_Z$	± 0.53	± 0.35	± 0.44
	(± 0.30)	(± 0.20)	(± 0.24)
λ_γ	± 0.79	± 0.77	± 0.83
λ_Z	± 0.47	± 0.37	± 0.44
$\lambda_\gamma = \lambda_Z$	± 0.44	± 0.29	± 0.36
	(± 0.25)	(± 0.16)	(± 0.20)

Table 3.7. Limits on anomalous couplings that could be set from $p\bar{p} \rightarrow W^\pm + 2 \text{ jets}$ with polarized or unpolarized protons, from events with $\sqrt{\hat{s}} > 340$ GeV. The numbers in parentheses are for 10 fb^{-1} integrated luminosity, and the other numbers are for 1 fb^{-1} integrated luminosity.

Parameter	Limits		
	$p(R)$	$p(L)$	Unpol
$\Delta\kappa_\gamma = \Delta\kappa_Z$	± 0.34 (± 0.19)	± 0.23 (± 0.13)	± 0.28 (± 0.16)
$\lambda_\gamma = \lambda_Z$	± 0.28 (± 0.16)	± 0.18 (± 0.10)	± 0.23 (± 0.13)

Table 3.8. Effect of parton Q scale on the calculated cross-section for background processes $p\bar{p} \rightarrow W^\pm + 2 \text{ jets}$. These are unpolarized cross-sections, calculated with CTEQ2 parton distribution functions.

Q scale	σ (pb)
$\sqrt{\hat{s}}$	$6.420 \pm .056$
$\sqrt{\hat{s}}/2$	$8.538 \pm .074$
$2M_W$	$7.398 \pm .068$

Figure Captions

Figure 1.1. Polarized parton distribution functions. The curves are $x\Delta f(x)$ vs x for parton types u_{val} , d_{val} , $u_{sea}(=d_{sea})$, g , which are the most important partons in our calculations.

Figure 2.1. Feynman diagrams for the process $u\bar{d} \rightarrow W^+\gamma$.

Figure 2.2. Total cross-section (with cuts in Eqs. (12)-(15)) for polarized protons vs anomalous coupling $\Delta\kappa_\gamma$, assuming $\lambda_\gamma = 0$. The unpolarized cross-section was calculated separately using CTEQ2 parton distribution functions.

Figure 2.3. Total cross-section (with cuts in Eqs. (12)-(15)) for polarized protons vs anomalous coupling λ_γ , assuming $\Delta\kappa_\gamma = 0$. The unpolarized cross-section was calculated separately using CTEQ2 parton distribution functions.

Figure 2.4. Distribution of photon transverse momentum $p_{T\gamma}$. The solid line is for $\Delta\kappa_\gamma = 0$, and the dashed line is for $\Delta\kappa_\gamma = -1$; in both cases $\lambda_\gamma = 0$.

Figure 3.1. Complete set of electroweak diagrams for $u + \bar{u} \rightarrow d + \bar{u} + W^+ (\rightarrow \bar{\ell} + \nu_\ell)$.

Figure 3.2. Two-jet invariant mass distribution for the signal process. The solid line is the result of the complete calculation of the pure electroweak process $p + \bar{p} \rightarrow q\bar{q}'W^+$, with $W^+ \rightarrow \bar{\ell}\nu_\ell$; the dotted line is the result of the calculation of W^+W^- production, with $W^+ \rightarrow \bar{\ell}\nu_\ell$ and $W^- \rightarrow 2 jets$, with a cut on the two-jet invariant mass ($70 < M_{2j} < 90$ GeV).

Figure 3.3. Two-jet invariant mass distribution for the QCD background processes $p\bar{p} \rightarrow W^+ + 2 jets$. (The cross-section for $W^- + 2 jets$ is the same, for unpolarized scattering.)

Figure 3.4. $\sqrt{\hat{s}}$ distribution for the signal process. The solid line is the result of the complete calculation of the pure electroweak process $p + \bar{p} \rightarrow q\bar{q}'W^+$, with $W^+ \rightarrow \bar{\ell}\nu_\ell$; the dotted line is the result of the calculation of W^+W^- production, with $W^+ \rightarrow \bar{\ell}\nu_\ell$

and $W^- \rightarrow 2 \text{ jets}$, with a cut on the two-jet invariant mass ($70 < M_{2j} < 90 \text{ GeV}$).

Figure 3.5. Comparison of $\sqrt{\hat{s}}$ distributions for signal and background processes. The solid line is the QCD background. The dotted line is the electroweak process, with zero anomalous couplings; the dashed line is the electroweak process with $\Delta\kappa_\gamma = \Delta\kappa_Z = 0.5$.

Figure 3.6. Comparison of $\sqrt{\hat{s}}$ distributions for signal and background processes, for $\sqrt{\hat{s}} > 340 \text{ GeV}$. The solid line is the QCD background. The dotted line is the electroweak process, with zero anomalous couplings; the dashed line is the electroweak process with $\Delta\kappa_\gamma = \Delta\kappa_Z = 0.5$.

Figure 3.7. Electroweak cross-section for $p_\lambda \bar{p} \rightarrow W^+ W^-$ as a function of anomalous couplings $\Delta\kappa$, for polarized (L, R) and unpolarized protons. For each polarization, three cases are shown, corresponding to assumptions (\times) $\Delta\kappa_\gamma \neq 0$ and $\Delta\kappa_Z = 0$, (\diamond) $\Delta\kappa_\gamma = 0$ and $\Delta\kappa_Z \neq 0$, and (\square) $\Delta\kappa_\gamma = \Delta\kappa_Z$. In all cases $\lambda_\gamma = \lambda_Z = 0$.

Figure 3.8. Electroweak cross-section for $p_\lambda \bar{p} \rightarrow W^+ W^-$ as a function of anomalous couplings λ , for polarized (L, R) and unpolarized protons. For each polarization, three cases are shown, corresponding to assumptions (\times) $\lambda_\gamma \neq 0$ and $\lambda_Z = 0$, (\diamond) $\lambda_\gamma = 0$ and $\lambda_Z \neq 0$, and (\square) $\lambda_\gamma = \lambda_Z$. In all cases $\Delta\kappa_\gamma = \Delta\kappa_Z = 0$.

Figure 3.9. Electroweak cross-section for $p_\lambda \bar{p} \rightarrow W^+ W^-$ as a function of anomalous couplings, with $\sqrt{\hat{s}} > 340 \text{ GeV}$. For each polarization, two cases are shown, corresponding to assumptions (\times) $\Delta\kappa_\gamma = \Delta\kappa_Z$ with $\lambda_\gamma = \lambda_Z = 0$, and (\diamond) $\lambda_\gamma = \lambda_Z$ with $\Delta\kappa_\gamma = \Delta\kappa_Z = 0$.

Figure 1.1

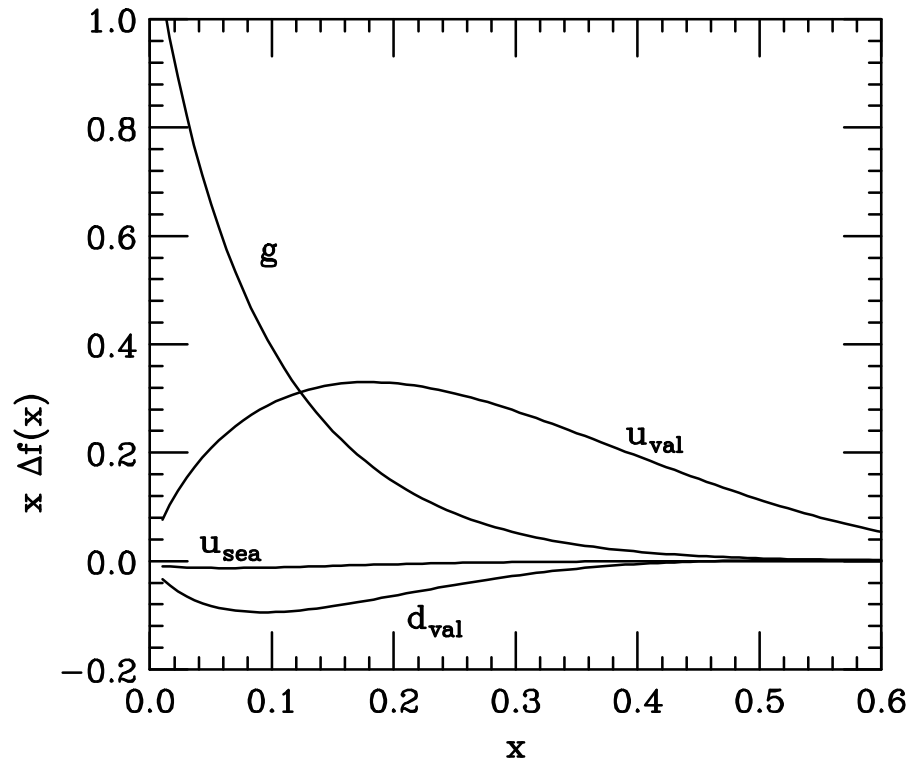


Figure 2.1

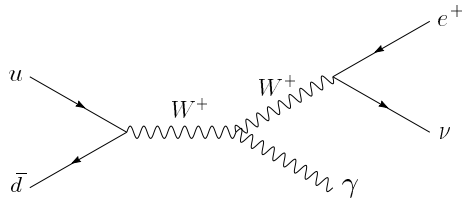
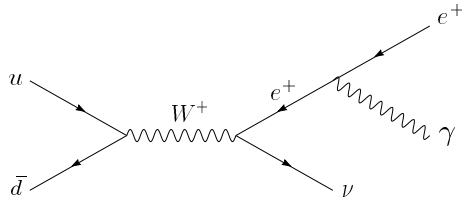
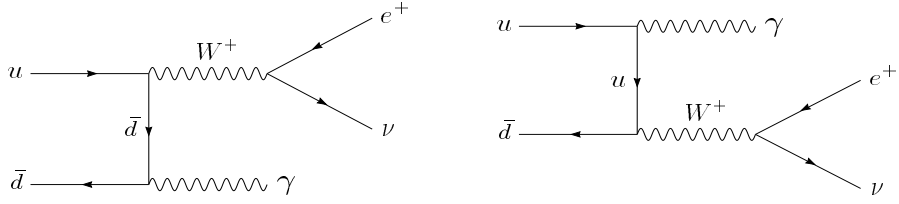


Figure 2.2

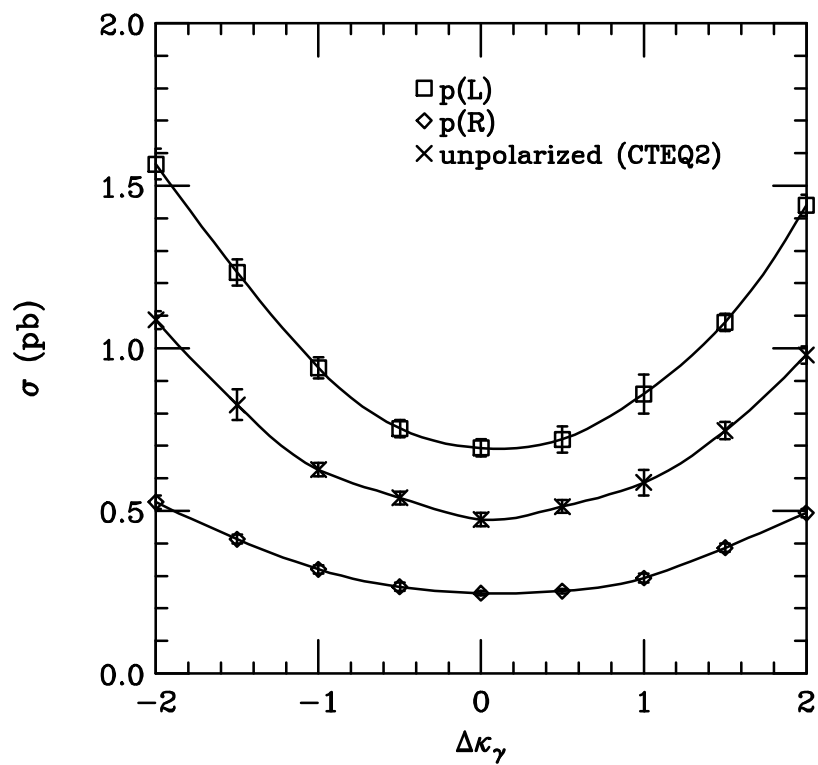


Figure 2.3

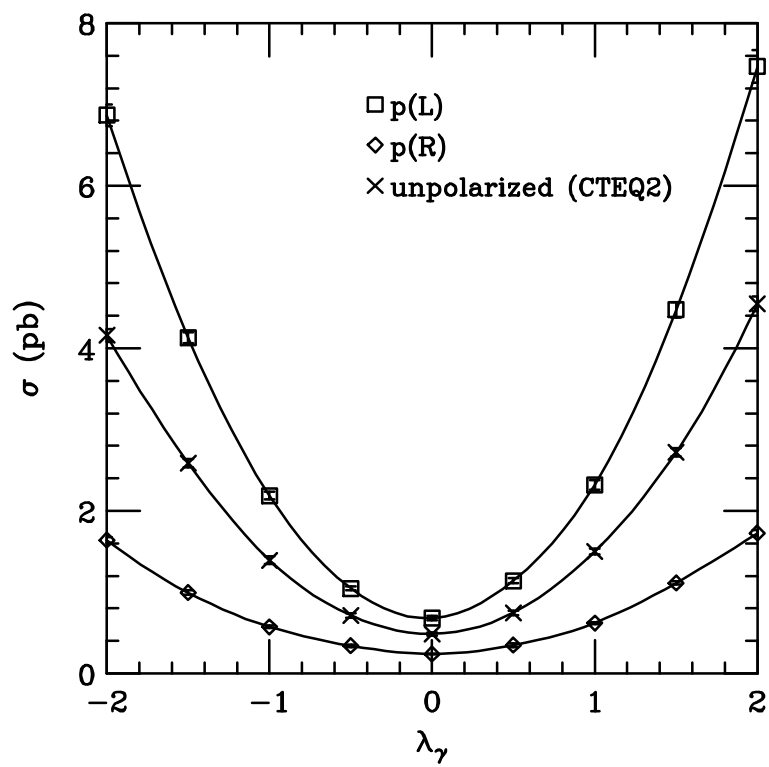


Figure 2.4

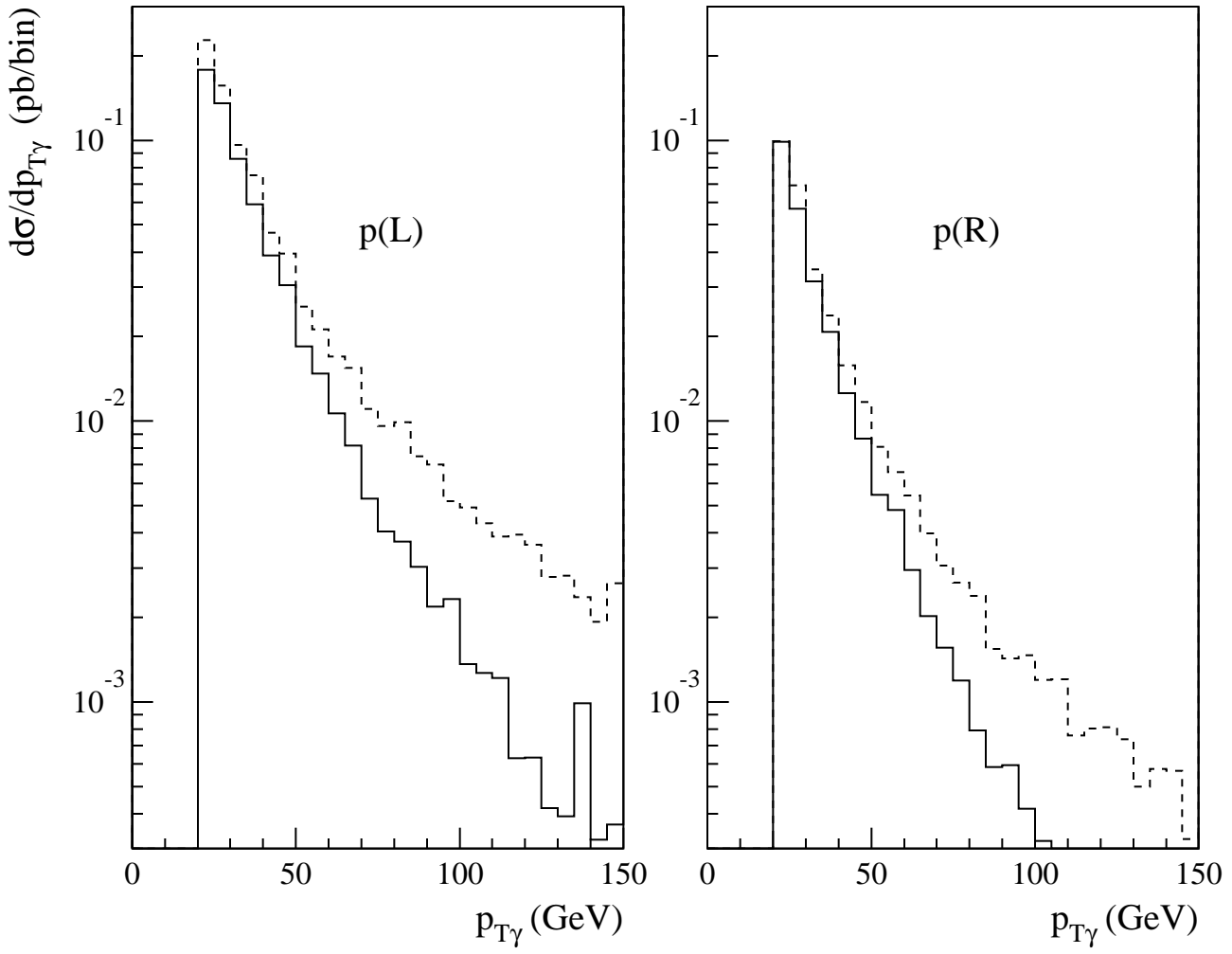


Figure 3.1

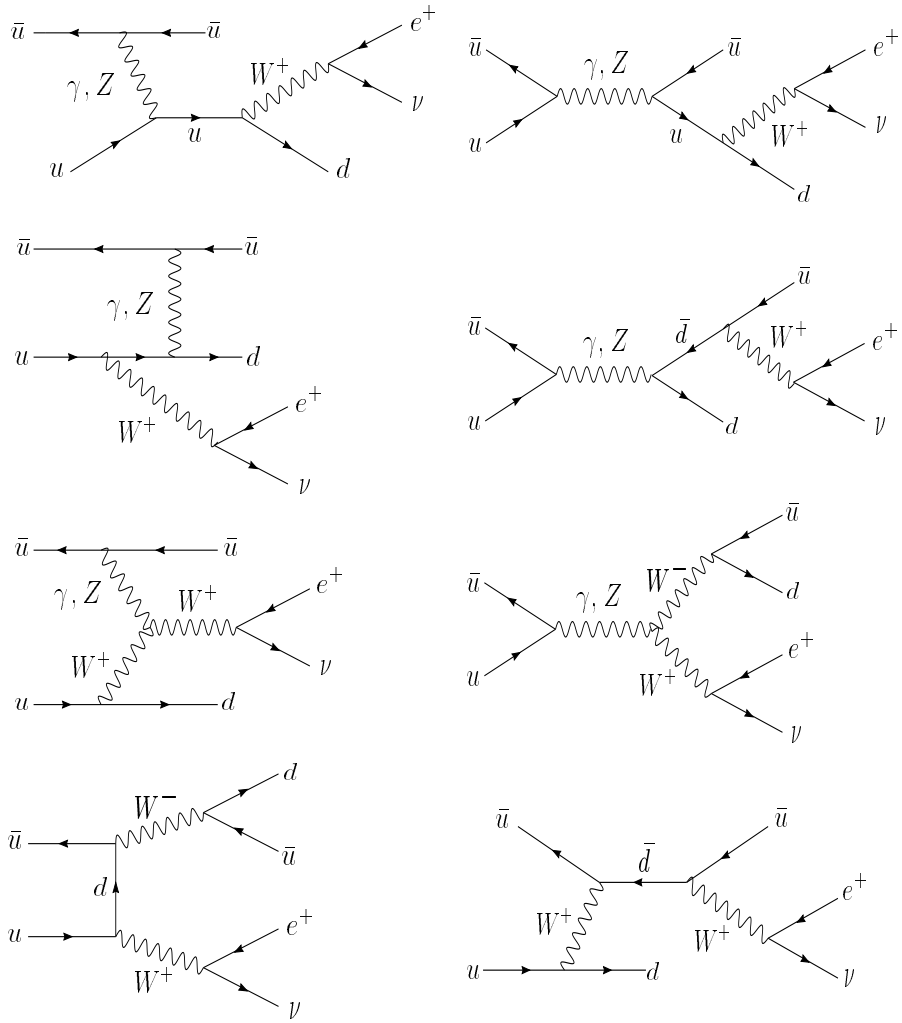


Figure 3.3

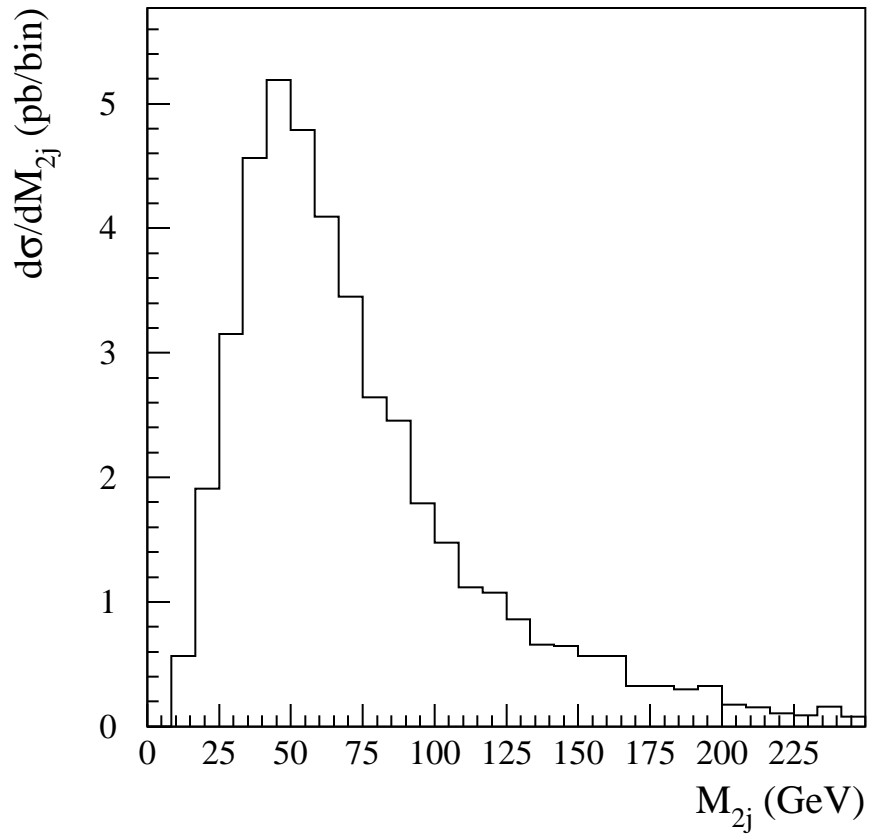


Figure 3.4

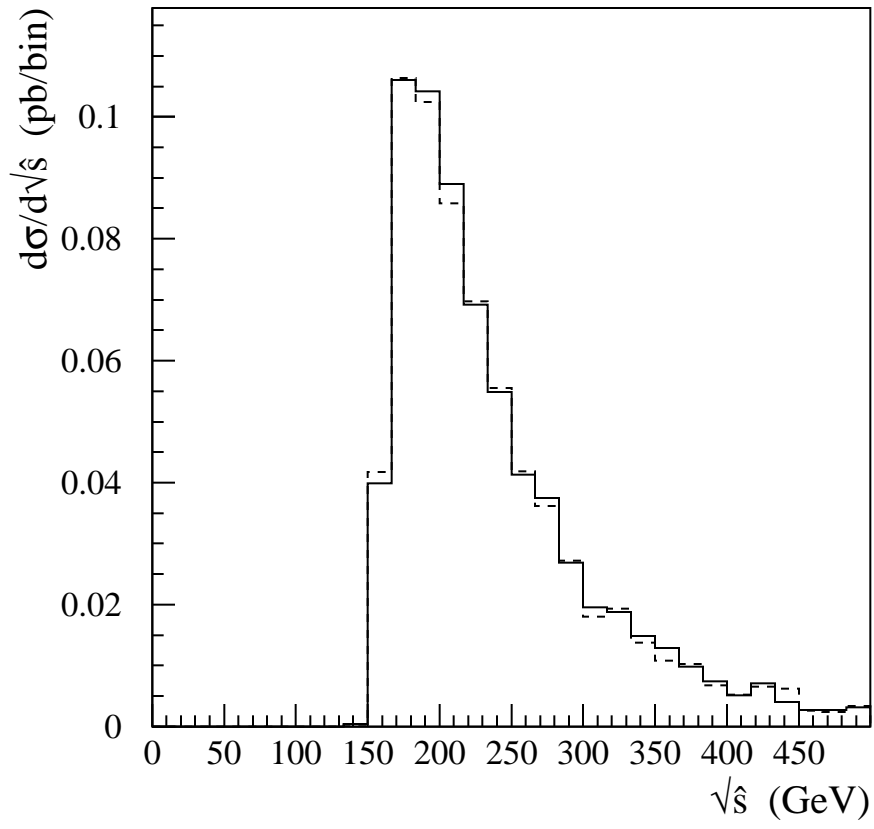


Figure 3.2

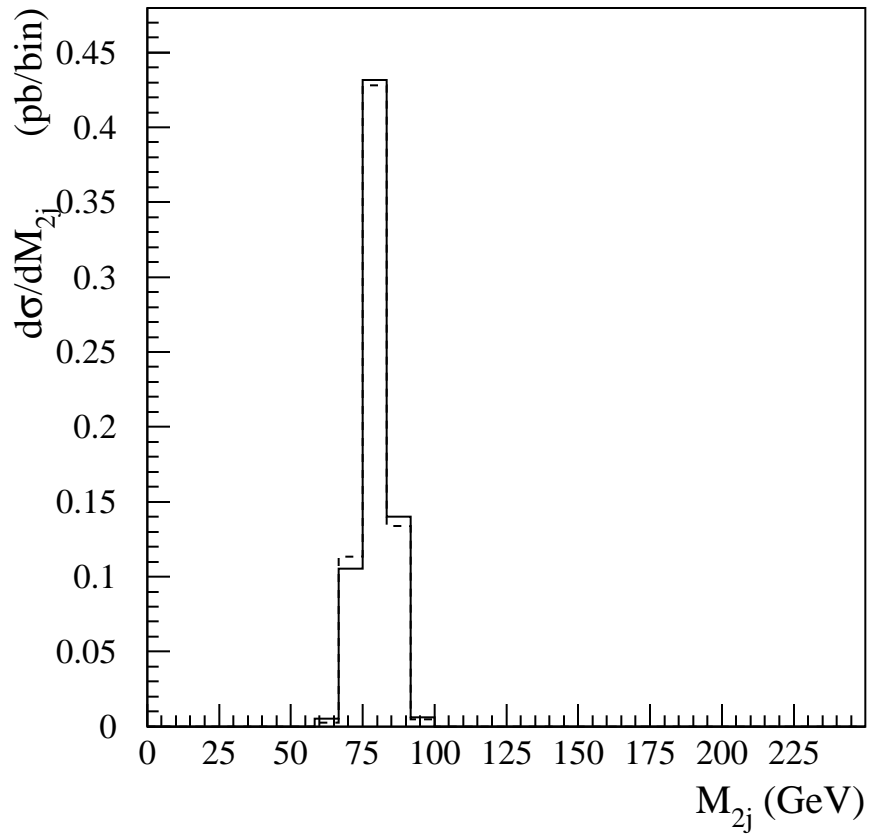


Figure 3.5

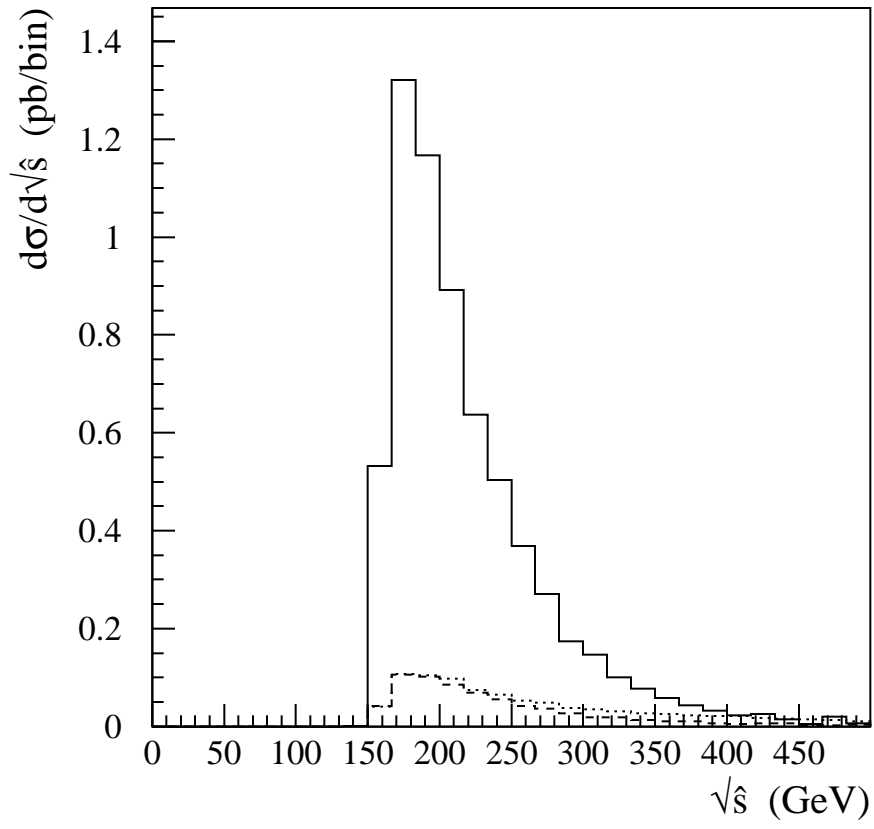


Fig 3.6 Signal vs. Background for $\sqrt{\hat{s}} > 340$ GeV

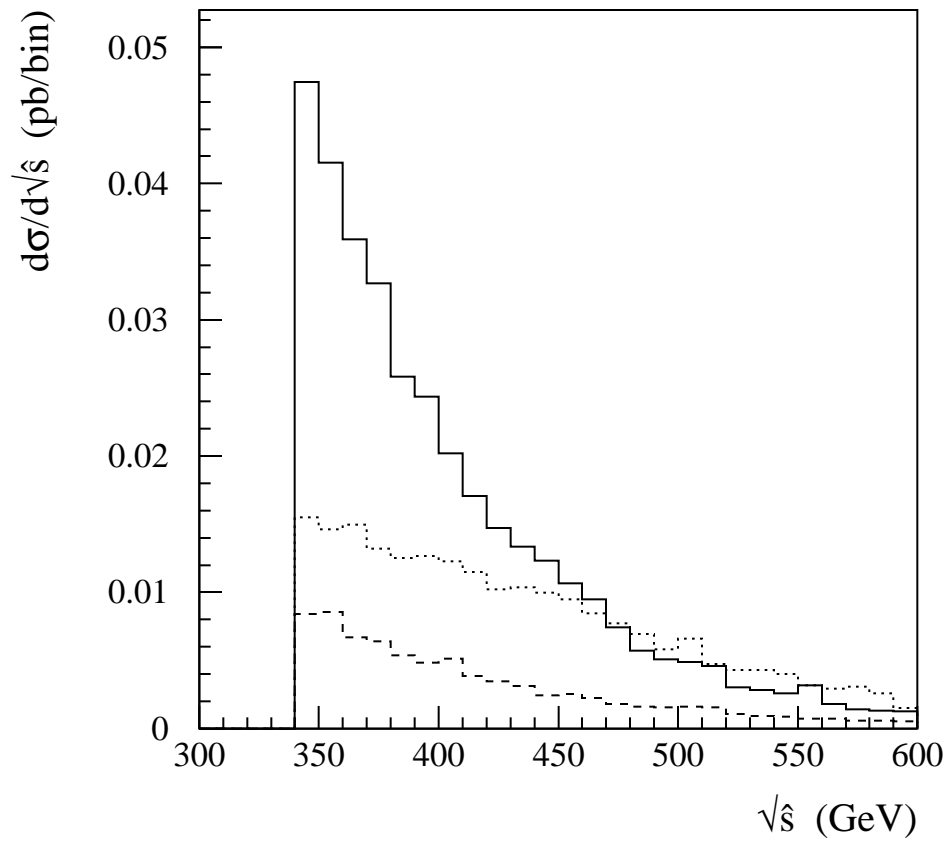


Figure 3.7

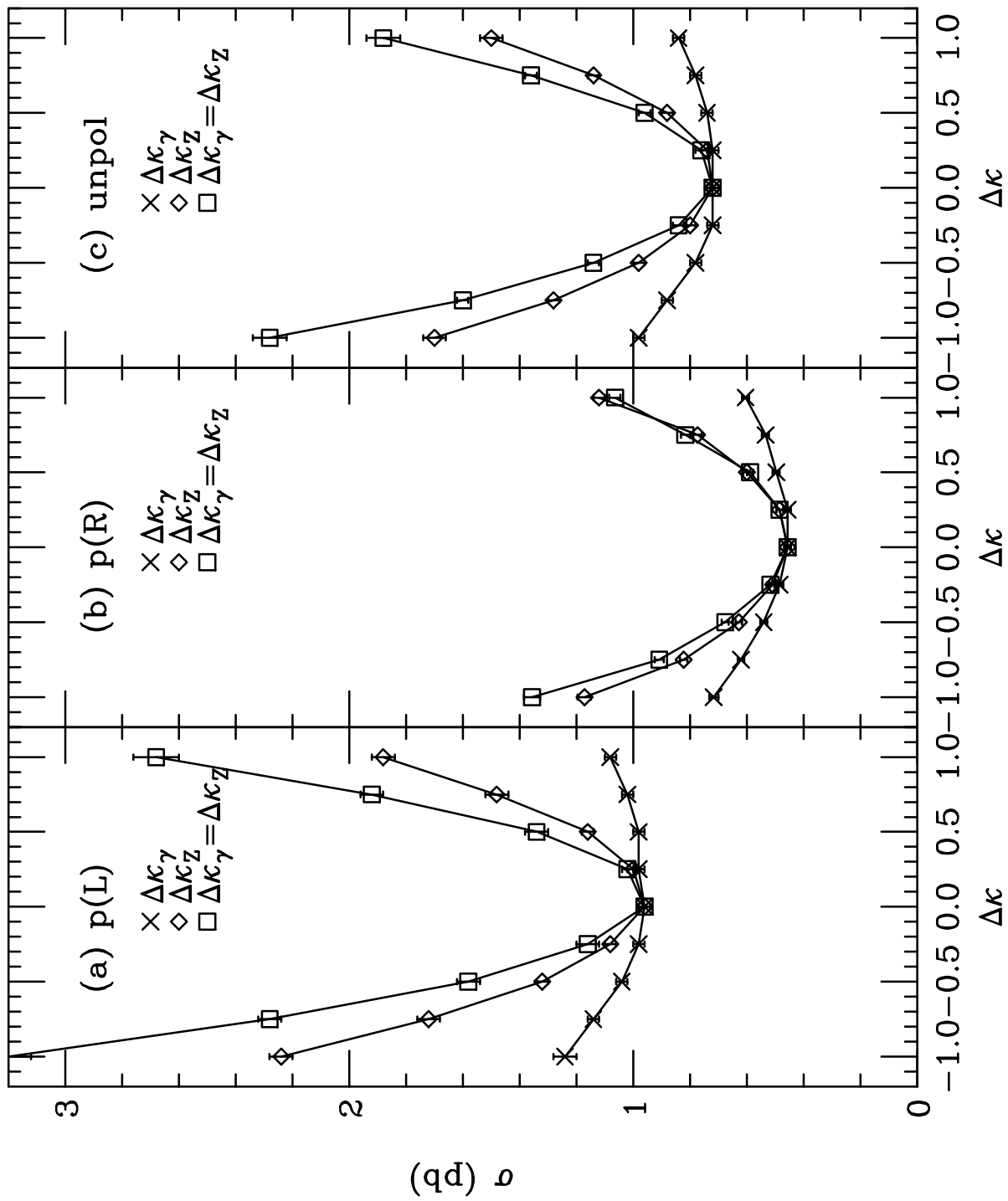


Figure 3.8

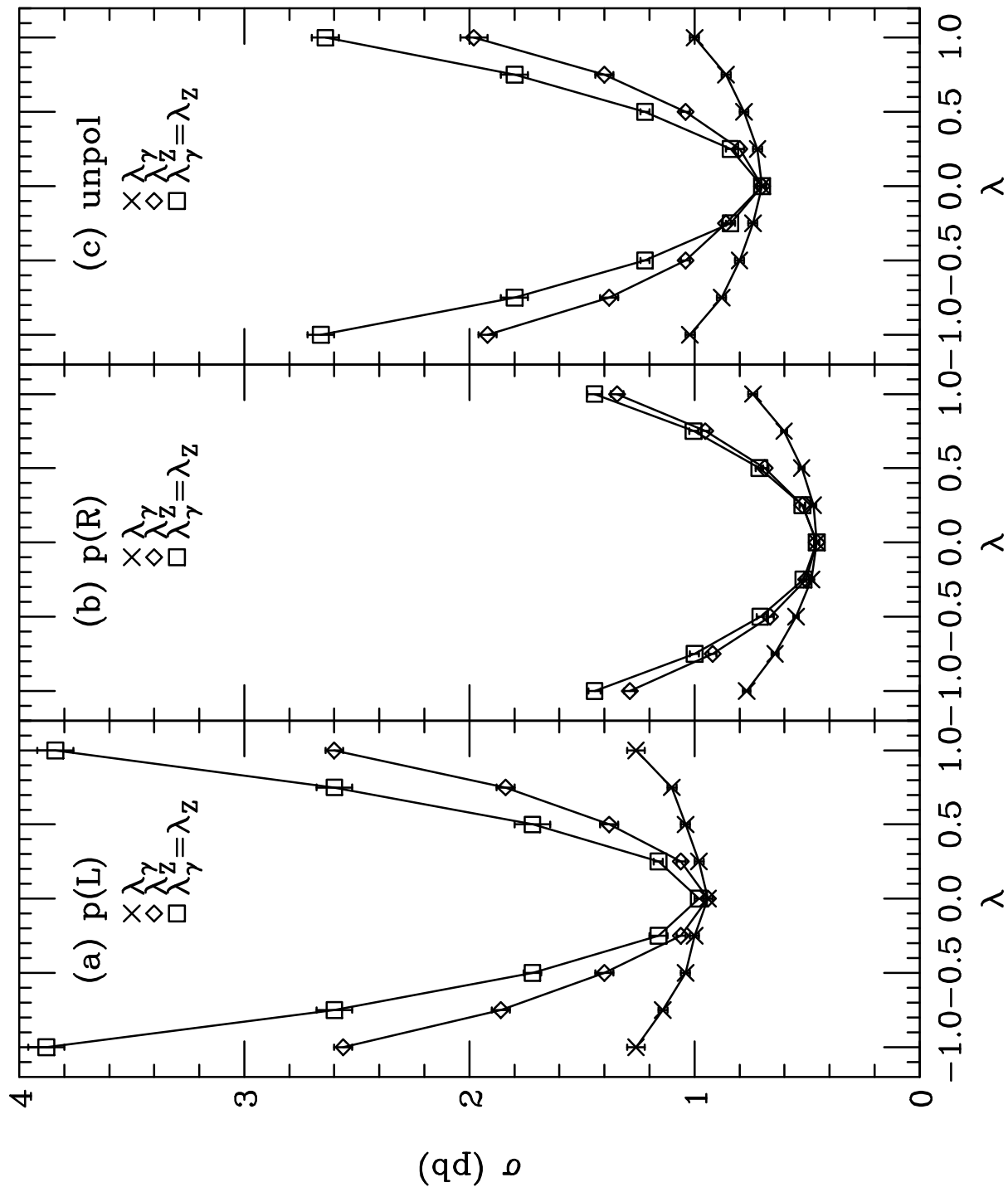


Figure 3.9

